Continental interior storm tracks, tritium deposition, and precipitation isotopes at the Great Basin-Rocky Mountain physiographic provinces transition zone, USA

Mayo, A.L.[1], and Tingey, D.G.[2]

[1] Mayo and Associates LC, Phoenix Arizona, alan_mayo@live.com
[2] Brigham Young University, Provo, Utah USA, dgtingey@gmail.com

Key Points

- The flux and isotopic composition of Southwestern United States continental interior precipitation are not correlatable with the El Niño-Southern Oscillation Oceanic Niño Index (INO).
- Tritium deposition is highly variable (2.1 to 29.5 TU) and is influenced by the four storm track trajectories, the 'spring leak', thunderstorms, and surface moisture evaporation.
- Most winter precipitation is isotopically depleted due to cold cloud temperatures and twenty-five percent is seasonally evaporated due to partial rain droplet evaporation.

Abstract

Thirteen years of precipitation δ^2H, $\delta^{18}O$, and ^3H data for three western United States continental interior weather stations, supplemented with 60 years of precipitation data, have been analyzed. The stations are located 1,000 to 2,000 km from four ocean moisture sources. Precipitation was evaluated relative to storm track trajectory, the El Niño-Southern Oscillation Oceanic Niño Index (INO), orography, precipitation amount, air temperature, month, and season. The INO was not fond to correlate with precipitation flux or isotopic composition. Tritium deposition was evaluated relative to the 'spring leak', thunderstorms, surface evaporation, storm tracks, and seasons. Local meteoric water lines and the Global Meteoric Water Line were compared. Winter precipitation is isotopically depleted and summer precipitation is isotopically enriched. Factors affecting the stable isotopes include winter cold cloud temperature, summer rain droplet partial evaporation, gradual rain out, and multiple episodes of soil moisture re-evaporation and subsequent re-precipitation.

1 Introduction

The isotopic composition of precipitation is of particular interest to hydrologic and hydrogeologic investigations. Beginning 1953, with the advent of atmospheric thermonuclear testing, the concentration atmospheric bomb ^3H overwhelmed the natural stratospheric ^3H. The long-lasting atmospheric ^3H spike provides a time maker in many water related investigations. Atmospheric bomb ^3H has been exhausted for the past 30 or so years due to the 'rain out' effect and more recent precipitation contains natural ^3H concentrations. The short 12.3-year half-life makes ^3H particularly useful for identifying recent groundwater recharge.

Stable isotopic molecules are often used to 'finger print' water, help sort out phenomena related to precipitation temperature such as climate, elevation and season, to identify evaporated water, and to characterize geothermal groundwater circulation. The study of the stable isotopic ratios $^2H/^1H$ and $^{18}O/^{16}O$ in natural waters began in the 1930's (Gilfillan, 1934; Harada, and Titani, 1935; Lewis and Cornish, 1933; Tes, 1939) and resumed in earnest after World War II (Craig et al., 1956; Dansgaard, 1953, 1954, 1964; Ehhalt et al., 1963; Epstein, 1956; Epstein and Mayeda, 1953; Friedman, 1953; Kobayakawa and Horibe, 1960). In his seminal paper Harmon Craig (Craig, 1961) analyzed 400 samples from worldwide locations of rivers, lakes, and precipitation

for the stable isotopic ratios. About 40 percent of the samples were from North America. The purpose of Craig's research was to establish the isotopic relationships of meteoric water. Except for evaporated water in closed basins, the plotted trend of the data is represented by the equation:

$$\delta^2H = 8\delta^{18}O + 10 \text{ ‰} \quad (1)$$

where δ^2H and $\delta^{18}O$ are the ratios of $^2H/^1H$ and $^{18}O/^{16}O$, respectively of the sample relative to Standard Mean Ocean Water (SMOW). SMOW is exhausted and the new standard is Vienna Standard Mean Ocean Water (VSMOW). Differences between samples and the standard are small and the differences are reported as permil rather than the more familiar percent. Eq. 1 was originally called the Craig Line and is now known as the widely used Global Meteoric Water Line (GMWL). In Eq. 1 the value 8 is the line slope and +10 is the deuterium intercept on the y axis. The y intercept is also known the deuterium excess. Craig found that the GMWL is consistent with Rayleigh liquid-vapor equilibrium distillation between -10 and 100 ^oC. Colder precipitation temperatures correspond to more negative isotopic values.

In 1964 Dansgaard (1964) analyzed 1,126 stable isotopic results from 84 worldwide International Atomic Energy Agency World Meteorological Organization (IAEA WMO) precipitation network stations. He found that local precipitation data commonly deviate from Rayleigh distillation in that both the line slope and the y intercept can vary greatly. The precipitation network included all continents, except for inland Asia, and numerous oceanic islands. Most of Dansgaard's stations were located near an ocean and each data set included at least one full year of measurements. Since 1964 it has been well documented that the stable isotopic composition of precipitation may be effected by geographic and meteorological factors including latitude, land surface elevation (altitude effect), distance from the coast (rain out effect), season, climate and paleoclimate, surface air temperature, precipitation intensity (amount effect), and storm tracks (Clark and Fritz, 1997; Gat, 2001; Merlivant and Jouzel, 1979; Rozanski et al., 1993; Siegenthaler and Oeschger, 1980; Yurtsever, 1975).

Temporal variability in stable isotopic compositions of precipitation have been used 1) to develop local meteoric water lines (Benjamin et al., 2004; Klaus et al., 2015; Yeh, 2014), 2) as proxies for past climate particularly as related to speleothem formation (Cross et al., 2015; Duan

et al., 2016; Pape at al., 2010), 3) to evaluate the amount effect (Easto and Dettman, 2016; Hager and Foelsche, 2015), 4) to evaluate interannual temperature changes (Bowen, 2008; Cai and Tian, 2016), and 5) to evaluate seasonal storm tracks (Araguás et al., 1998; Kurita et al., 2014; Vuille amd Wermer, 2005). Precipitation stations located in mid-continental settings commonly have seasonal isotopic variations (Gat, 2001; IAEA, 2021). For example, in Vienna, Austria and Ottawa, Canada the average seasonal variations in $\delta^{18}O$ are as great as 18‰ between winter and summer precipitation. Based on a limited data set Benjamin et al. (2004) found several per mil variability in $\delta^{18}O$ between winter and summer precipitation events at a single station in the interior of the western United States.

Of interest here are the isotopic compositions of precipitation at the Great Basin-Rocky Mountain physiographic provinces transition zone in the interior of the southwestern United States (Fig. 1). The bomb tritium spike in the interior of the southwestern US is well documented in IAEA (2021) data. Benson and Klieforth (1989) measured seasonal stable isotopic variations in southern Nevada, Friedman et al. (1992) and Smith et al. (1992) investigated stable isotopic compositions of precipitation in southern California, and Friedman et al. (2002a) investigated air mas trajectories using 3 years of data (1991-1993) from two locations. Houghton (1979 investigated orographic effects, Friedman et al. (2002b) evaluated spatial stable isotopic trends using seasonal data (1991-1996) from continuous collectors at 41 stations, and Benson (2017) investigated precipitation in the southwestern portion of the Great Basin.

The purpose of this investigation is to better understand the meteorological and orographic factors that affect the isotopic compositions of precipitation in the interior of the western United States. We have analyzed the isotopic compositions of precipitation from three stations at the transition between in the northeastern Great Basin and the Rocky Mountain physiographic provinces (Fig. 1). The three Utah transition zone locations were selected for study because they potentially receive precipitation from the same storm tracts, yet have very different orographic characteristics. One station, Pilot Valley-Silver Island Range, is located in the Great Basin about 190 km west of the Great Basin-Rocky Mountain transition. One station, Lindon, Utah, is located at the transition between the two physiographic provinces at the base of the Wasatch

103 Range. One station is located on the Wasatch Plateau near the top of the Wasatch Range in the
104 Rocky Mountain physiographic province.

105

106 Figure 1 Location of precipitation collection locations in the Great Basin. The Great Basin is a
107 vast region of internal drainage in the western United States is the northern portion of the
108 Basin and Range physiographic province. The Wasatch Range marks the eastern
109 boundary of the Great Basin and separates the Great Basin from the Rocky Mountain
110 physiographic province to the east.

111 2 Data and Methodology

112 Two years of data (2005-2007) were developed for eight cumulative collection stations in Pilot
113 Valley (Fig. 1). The stations were collected monthly and included 133 stable isotope and five ^{3}H
114 samples. The cumulative collectors were treated with a layer of oil to prevent evaporation. The
115 Pilot Valley stations are located on the western Silver Island Range alluvial fan (windward side).

The stations range in elevation from 1,300 m above mean sea level (amsl) on the valley floor to 1,650 m amsl on the Silver Island Range alluvial fan, and were located ~3.5 to 5 km west of the range ridge line. Thirteen years (1999 - 2012) of daily precipitation samples were collected at the Lindon station. Analysis included 335 δ^2H and $\delta^{18}O$ and 79 ^3H samples. The Lindon station is located at the base of the Wasatch Range on the very edged of the northeastern Great Basin at an elevation of 1,445 m amsl. The Wasatch Range rises to 3,582 m amsl about 7 km east of the station. One year of bi-weekly snow and rain samples (1999-2000) were collected from the two Wasatch Plateau stations. One station was at 2,682 m amsl and one was at 2,877 m amsl. Snow was collected from the top layer of the snow pack and allowed to thaw in sealed containers and rain was obtained from two oil treated continuous collectors. The plateau is located about 40 km east of the eastern edge of the Great Basin.

Laboratory analyses were performed at Brigham Young University facilities. The stable isotopes were analyzed using a Finnegan Delta Plus mass spectrometer and the tritium samples were electrolytically enriched prior to analysis with a 1220 Quantulus ultra low-level liquid scintillation spectrometer. $\delta^{18}O$ and δ^2H measurements are ± 0.3 and 1.0 ‰, respectively, and the ^3H minimum detection limit (MDL) is 0.3 TU.

Storm tracks for each Lindon station sampling date were determined using the National Oceanic and Atmospheric Administration (NOAA) program HYSPLIT (NOAA, 2021). Stable isotopic data were statically compared to the GMWL by creating a synthetic GMWL data set for the local data. The synthetic GMWL data was developed by calculating a δ^2H for each laboratory $\delta^{18}O$ value using Eq. 1. The synthetic δ^2H data and the laboratory data for each sample were then statically compared at the 95 percent confidence level.

Salt Lake City station ^3H data for 1963-1984 was obtained from the IAEA Global Network of Isotopes in Precipitation (GNIP) electronic data base (IAEA, 2021). The 230 Salt Lake City samples were from bi-weekly sampled continuous collectors. The Salt Lake station is located 50 km north of the Lindon station and occupies the same orographic position at the base of the Wasatch Range as the Lindon station. Precipitation amount data from the Wendover, Pleasant Grove, and Fairview weather stations (WRCC, 2021) were analyzed as surrogates for long-term Pilot Valley, Lindon, and Wasatch Plateau station data, respectively. The surrogate stations are

145 located within a few km of the study area stations and occupy similar physiographic and
146 orographic positions.

147 The tritium and stable isotopic data for Pilot Valley, Lindon and Wasatch Range stations has
148 been reported to the IAEA for inclusion in the GNIP data base and are available online.

149 Pilot Valley, Lindon and Wasatch Plateau stable isotopic and tritium data developed as part of
150 this research, and Salt Lake City tritium data are archived with the IAEA Global Network of
151 Isotopes in Precipitation (GNIP) electronic data base (IAEA, 2021). Wendover, Pleasant Grove
152 and Fairview, Utah precipitation data are available from the (WRCC, 2021).

153 # 3 Great Basin Orography, Storm Tracks, and Climate

154 The Great Basin, a 541,700 km^2 endorheic region, occupies the northern portion of the Basin and
155 Range physiographic province (Fig. 1). The Basin and Range is characterized by extension fault
156 block mountain ranges and valleys. The Great Basin contains more than 100 valleys, bounded
157 by more than 130 named north to northeast trending high mountain ranges, mountains, and hills
158 that have been described as aligned like a march of caterpillars. The mountain ranges are 95 to
159 190 km long and 5 to 24 km wide, and the valleys are commonly wider. The Silver Island
160 Range, an easternmost Great Basin mountain range, rises to 2,260 m amsl and is 960 m above
161 the adjacent Pilot Valley basin. The Wasatch Range marks the transition between the Great
162 Basin to the west and the central Rock Mountain physiographic province to the east. The range
163 rises as much as 2,500 m above the valley floors to the west. The range runs about 260 km from
164 the border with Idaho in the north to south-central Utah in the south. Although the Wasatch
165 Range is part of the Rocky Mountain physiographic province, the range drains into and is the
166 largest Great Basin watershed. The Wasatch Plateau, located in the central Wasatch Range, has
167 an average elevation of 2,690 m amsl.

168 Storms reaching the northeastern Great Basin-Rocky Mountain transition zone are carried along
169 four different air mass trajectories (Houghton, 1969; Friedman et al., 2002a). The trajectories
170 are: 1) cold polar air originating in the Artic, 2) the western flow of cool North Pacific Ocean air,
171 3) the northwestern flow tropical Pacific Ocean air, sometimes known as the Pineapple Express,
172 and 4) the northern flow of tropical Gulf of California-Gulf of Gulf of Mexico air (Fig. 2). The

air masses originate at ocean sources 1,000 to 2,000 km from the transition zone. Examples of individual storm tracks are shown on Fig. 3. Artic air peaks in the winter and is not a factor in the summer (Fig. 4). North Pacific air peaks in the winter and early spring, and tropical Pacific, and Gulf of California-Gulf of Mexico air peaks in the summer. Gulf of California-Gulf of Mexico air is often associated with the North American Monsoon (NAM) which provides warm moist air that provides the moisture for most mid-summer to early fall thunderstorms. The influence of the Great Basin on air masses varies greatly by trajectory. During the study period the percentage of storm carrying air mass trajectories that cross the Great Basin before reaching the Lindon station vary by source area: Artic 16 percent, North Pacific 87 percent, tropical Pacific 44 percent, and Gulf of California-Gulf of Mexico 7 percent. It was not possible to make similar calculations for the Pilot Valley and Wasatch stations, because the precipitation at these stations was collected using continuous collectors that were not monitored daily. It is likely that the Wasatch Plateau station has similar percentages of storm air mass trajectories crossing the Great Basin as the Lindon station. Almost all Pilot Valley storms must cross some or all of the Great Basin.

Air masses traversing the Great Basin rapidly undergo numerous adiabatic cooling and heating cycles as the air rises and falls when crossing the relatively narrow mountain ranges. Frequently storms traverse the Great Basin in 36 hours or less (Fig. 3). Assuming average winter and summer Great Basin adiabatic laps rates of 3.8 and 6.5 ^{o}C/km (Patrick, 2014; Dobrowski et al., 2009) and the average mountain block relief is 1 km, the near surface air would cool and heat several ^{o}C each time it crosses a mountain range. The heating and cooling results in increased precipitation at high mountain block elevations and more arid conditions in the valley floors. Average annual valley floor precipitation can be as small as 15 cm and mountain peak precipitation can be as great as 70 cm (Jeton et al., 2005; McEvoy et al., 2014). The net effect of this cooling and heating on the isolated mountain ranges are twofold: 1) the ranges are small, snow-pack dominated water sheds that are subject to interannual and decadal precipitation variability, and 2) precipitation falling on the ranges and valleys are subject to the isotopic elevation and rain out effects. Air masses that do not cross the Great Basin also undergo adiabatic changes but less frequently.

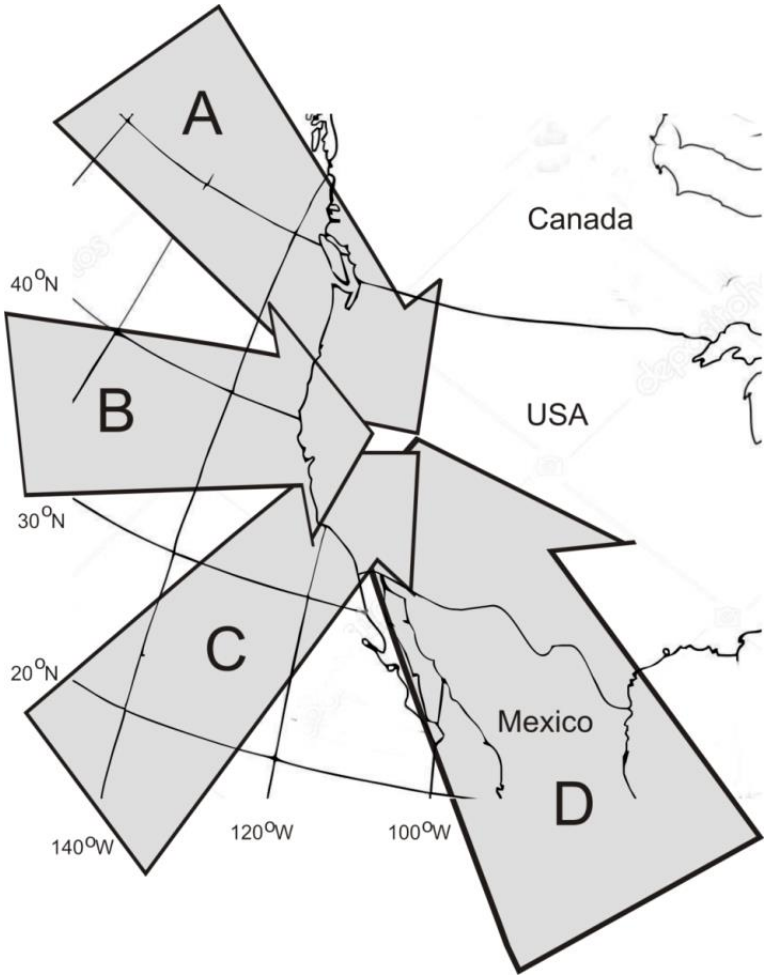

Figure 2 Storm tracks that provide moisture to the northeastern portion of the Great Basin: A) polar Artic air, B) cool, north Pacific Ocean air, C) tropical Pacific ocean air, and D) summer monsoon Gulf of California and Gulf of Mexico air. Continental summer thunderstorm air usually tracts from the west across the Great Basin.

a) North Pacific storm track (November 30-December 1, 2001)

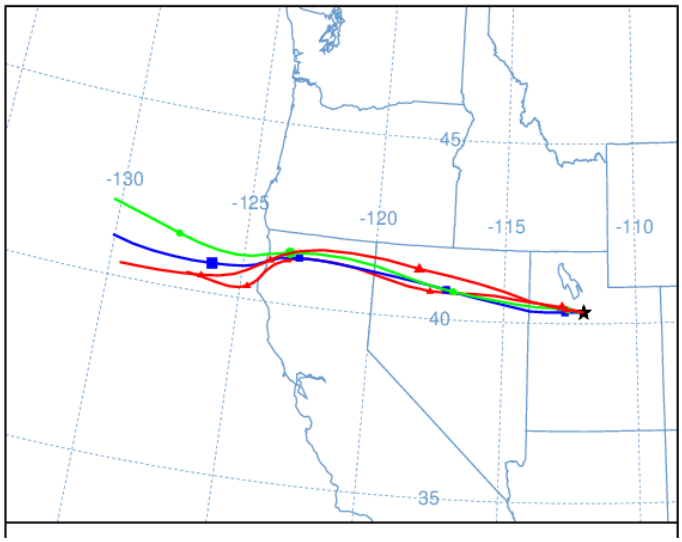

b) Tropical Pacific Storm Track (December 31-January 1, 2005)

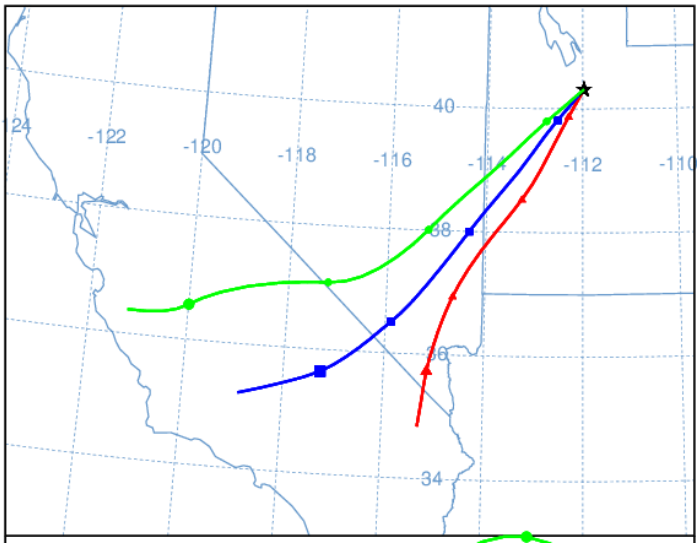

Fig. 3 Examples of NOAA HYSPLIT calculated 24 hour storm tracks reaching the Lindon station. North Pacific storms cross the Great Basin about 87 percent of the time and only about 44 percent of tropical Pacific storms cross the southern portion of the Great Basin. The symbols on the air mass trajectories represent 6-hour intervals.

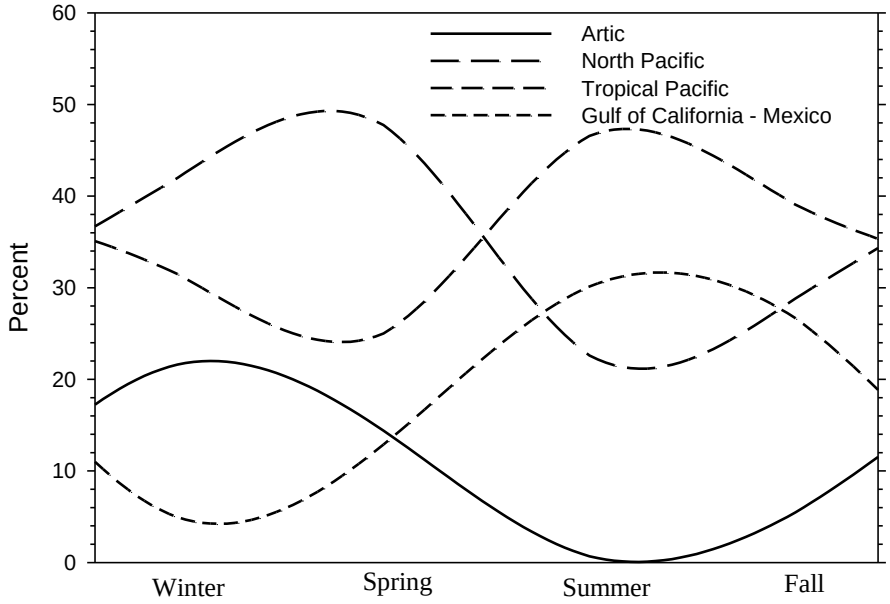

Fig. 4 Storm tracks associated with isotopic sampling events.

The Wasatch Range forms a physiographic barrier that influences and deflects storm tacks from the north, west, and south. Once the air mass ascends the Wasatch Range the air remains cool for an extended period of time as it passes over the relatively high and wide mountains and valleys of the range. Most tropical Pacific and Gulf of California-Gulf of Mexico air masses first reach the southern end of the Wasatch Range and then are funneled northward along the western side of the range before reaching the Lindon Station at the north end of the range. Tropical Pacific storms that cross the Great basin only skirt the southernmost portion of the basin, whereas North Pacific air masses typically cross entire Great Basin.

In addition to the storm track trajectories Great Basin and transition zone precipitation can be affected by the complex interaction of the El Niño-Southern Oscillation (ENSO), the Pacific Decadal Oscillation (PDO), and other Pacific Ocean atmospheric and ocean sea surface temperature (SST) trends (Mantua and Hare, 2002; Smith et al., 2015). ENSO impacts global atmospheric circulation including temperature and precipitation and has patterns that persist for 6 to 18 months. ENSO has three phases El Niño, Neutral, and La Niña. The severity of the phases is measured by NOAA using the Oceanic Niño Index (ONI). ONI is the 3-month running

average change in SST at the equator between 120° W and 170° W. El Niño occurs when the tropical Pacific Ocean is warmer and the index is +0.5 °C or higher than the 30-year average. La Niña occurs when tropical Pacific Ocean is cooler and the index is -0.5 °C or lower than average. Neutral is when the index is between +0.5 and -0.5. El Niño causes the Pacific jet stream to move south and La Niña cause the jet stream to move north. Unlike ENSO, PDO events persist for 20-30 years and mostly affect the North Pacific and adjacent North America. PDO is a measure of decadal trends in North Pacific Ocean SST.

The northern Great Basin is located at the ENSO forced winter weather transition boundary. The boundary is also known as the ENSO dipole or North American dipole. South of the transition a winter El Niño typically results in wetter conditions in the southwestern US and warmer and dryer conditions than usual north of the transition (Wang et al., 2012). La Niña is the opposite. Coupling of the ENSO dipole with the Pacific Decadal Oscillation (PDO; Mantura and Hare, 2002) other Pacific Ocean atmospheric and SST oscillations can shift the North American dipole to the north and to the south, thus greatly effecting northern Great Basin and transition zone precipitation rates, precipitation sources, and air temperatures (Brown, 2011; Smith et al., 2015; Wise, 2010). The net effect of this shift is wet and dry cycles of varying durations.

4 Analysis and Discussion

4.1 Precipitation

The climate at the three sampling stations progresses from semi-arid desert in Pilot Valley to humid continental (Step) in the Wasatch Plateau. At the Lindon and Wasatch Plateau stations winter is wet and cold, spring and fall are wet with variable temperatures, and summer is generally warm and dryer (Fig. 5). Much of the precipitation at the Wasatch station accumulates as snowfall. Snow accumulation is variable at the Lindon station and is infrequent at the Pilot Valley station. Pilot Valley precipitation usually peaks in the spring and early summer.

Based on an analysis of 60 years of Pleasant Grove monthly and annual precipitation data (1960-2020), there is no correlation between ENSO conditions and the average monthly and average storm total precipitation (Figs. 6 and 7). ONI index values were statically compared to Pleasant Grove monthly, 3-month running averages (732 events), and cumulative storm event totals

(1,108 events). The R^2 values of the correlation of the ONI vs. Pleasant Grove data range from 0.001 to 0.00003. An R^2 of 0.001 means that only 0.1 percent of the precipitation variability can be explained by the ONI index. There is also no correlation between long-term Wendover, UT (1960-2016), and Fairview, UT (1975-2010) precipitation data with ONI data. The R^2 values for the Wendover and Fairview data are 0.012 and 0.00012 respectively. Except for the Pleasant Grove February El Niño vs. neutral and vs. La Niña, and the December El Niño vs. La Niña storm event averages, there are no statistical differences between the ONI and either the monthly or storm event total precipitation amounts. The absence of correlation between the long-term precipitation data and ONI index means that the index is not a reliable predictor of transition zone precipitation or for use as a standalone tool for assessing transition zone precipitation isotopic data. Smith et al. (2015) simulated the effects of ENSO and PDO on Great Basin precipitation and found that ENSO over predicted and PDO under predicted precipitation. The lack of correlation between the ONI index and transition zone precipitation may be related to north and south migration of the North American Dipole.

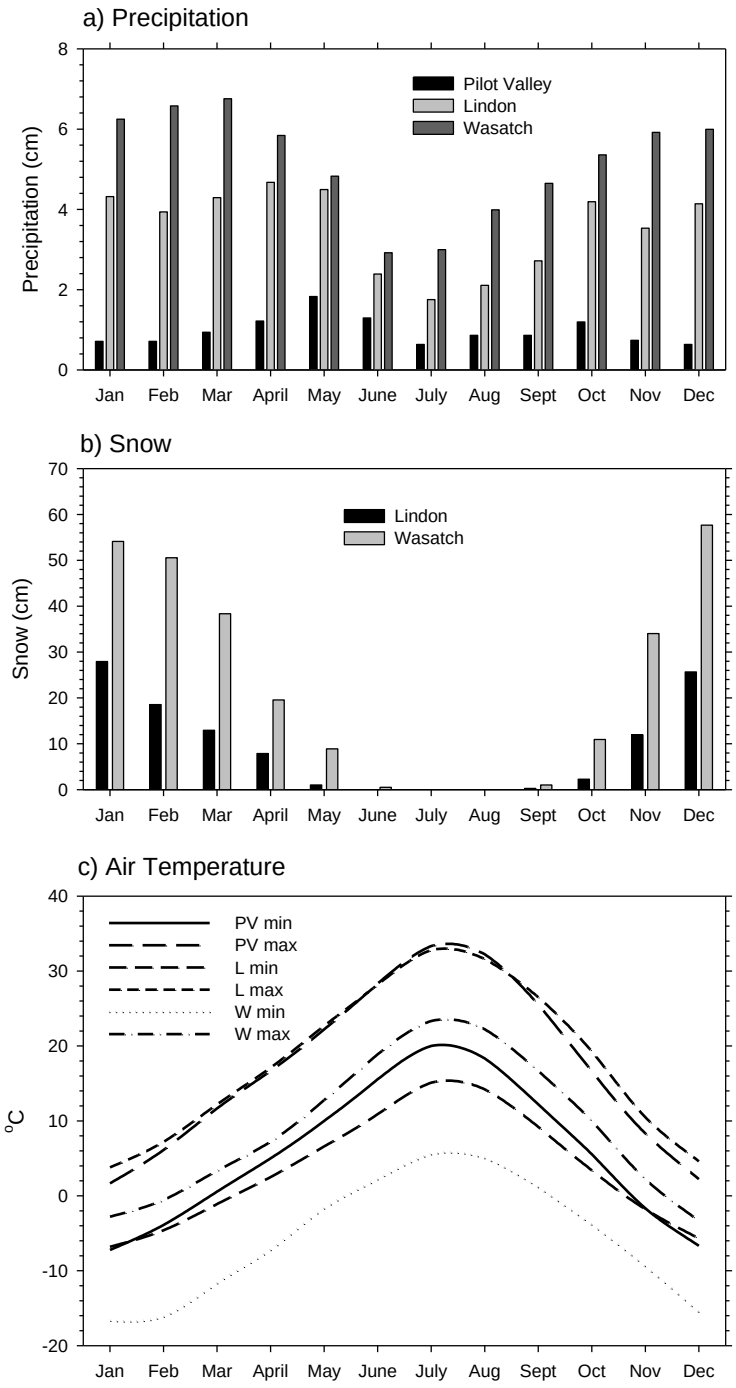

281

282 Fig. 5 Climate summary for Pilot Valley (PV), Lindon (L) and Wasatch Range (W) sampling
283 stations. Data are 40 year averages.

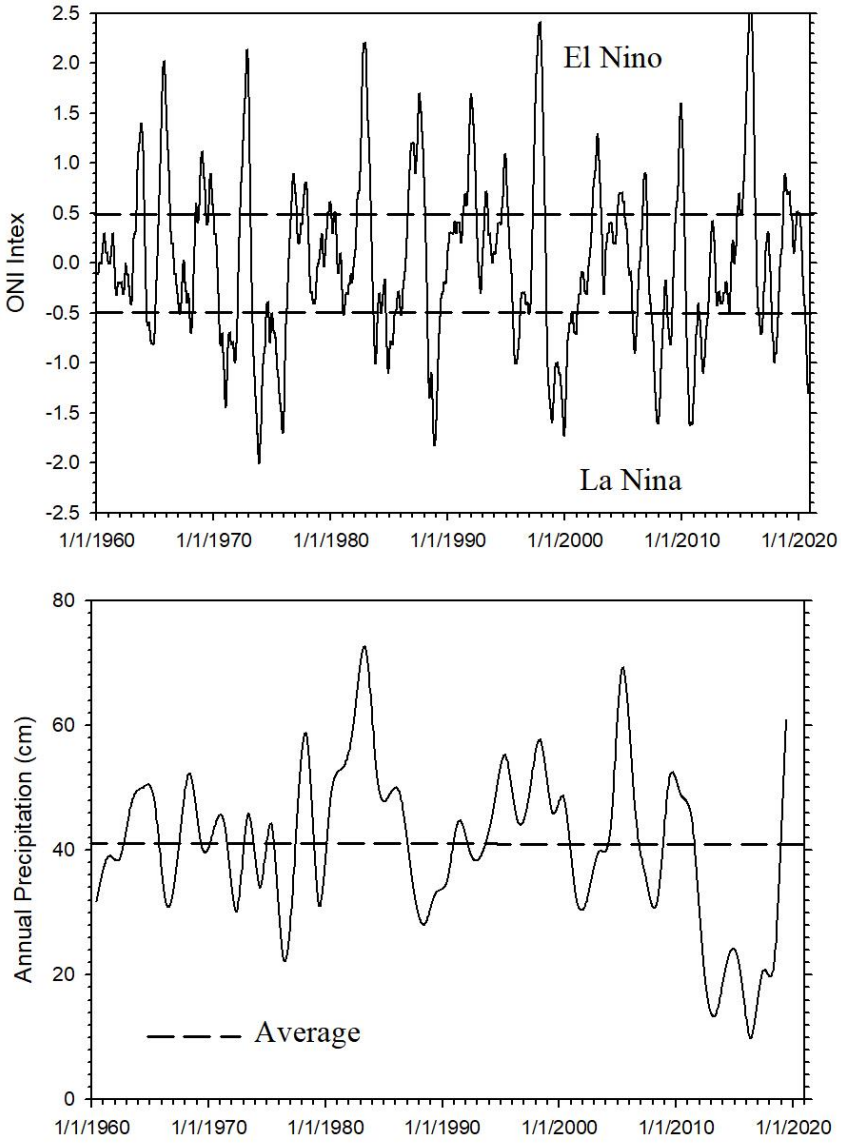

284

285 Fig 6 Comparison of ONI index and Pleasant Grove average annual precipitation.

286

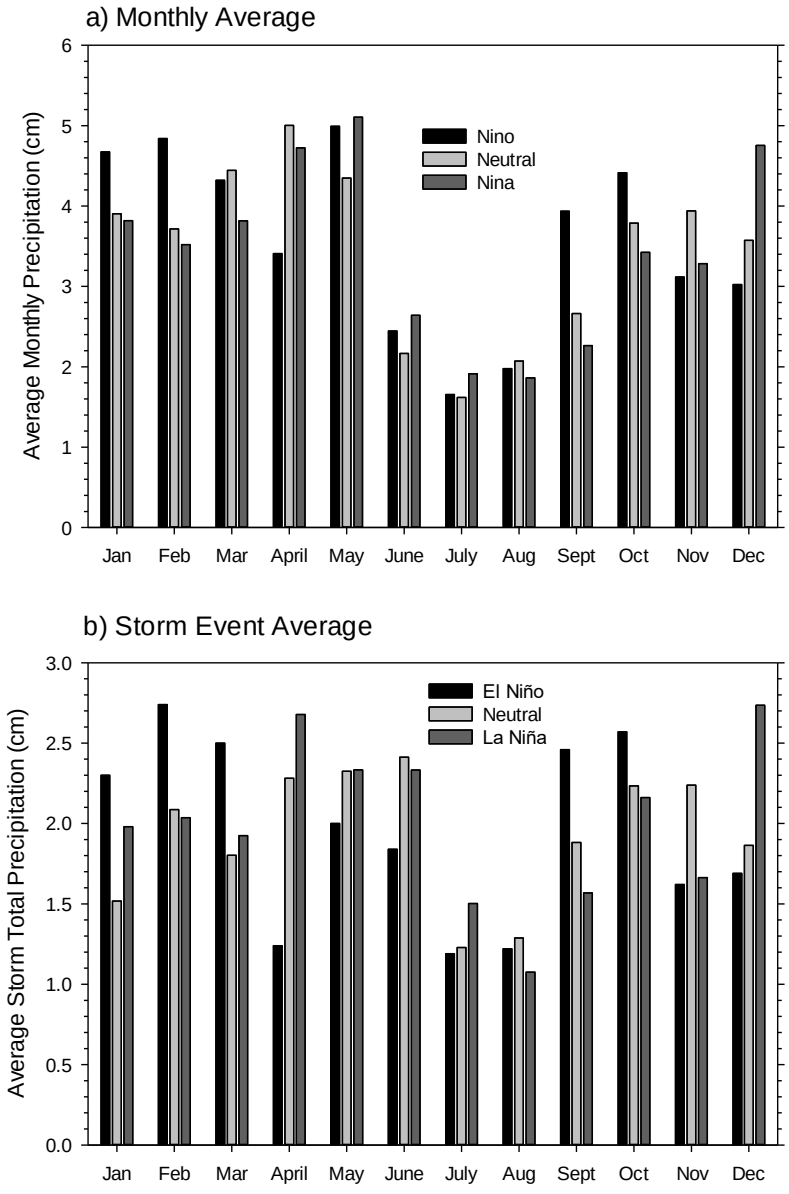

287

288 Fig. 7 Average Pleasant Grove station monthly total and storm event precipitation between 1960
289 and 2020.

290 **4.2 Tritium Deposition**

291 Transition zone tritium deposition has been measured at both the Salt Lake City and Lindon
292 stations (Fig. 8). The Salt Lake City data reflect the rain out effect after the cessation of
293 atmospheric thermonuclear testing in 1963. In 1963 individual storm events contained as much
294 as 10,000 TU. By 1994, at that end of the Salt Lake City sampling, the atmosphere contained
295 near natural atmospheric ^{3}H concentrations. The Lindon data represent natural atmospheric ^{3}H

deposition. The average and median ^{3}H concentrations of the Lindon precipitation are 8.5 and 7.6 TU, respectively, and the minimum and maximum concentrations are 2.1 and 29.5 TU. The standard deviation is 4.8 TU. The limited number of Pilot Valley samples had similar concentrations as the bulk of the Lindon samples. The ^{3}H concentrations in Lindon and Pilot Valley precipitation varied greatly between 2002 and 2012. There is no correlation between Lindon ^{3}H concentrations and precipitation amount or temperature, but there are statistical differences between the spring (March-May) and fall (September-November) data (Fig 9a), and between the Gulf of California-Gulf of Mexico storm tracks with the North Pacific and Artic storm tracks (Fig 9b). Factors that influence the concentration variability in natural tritium deposition and the statistical differences are discussed below.

Natural tritium is produced in the lower stratosphere and upper troposphere by the bombardment of cosmic rays. This tritium is rapidly removed as atmospheric water vapor only has a residence time of 10-30 days. Coastal precipitation typically has low tritium concentrations due to the exchange of atmospheric water vapor with the low tritium concentrations in ocean surface water (Schell et al., 1970; Suess, 1970). When storm systems move inland (continental effect) troposphere tritium concentrations increase by varying amounts as tritium deposition is affected by the timing and flux of stratosphere-troposphere exchange, and by near land surface processes. Processes that increase tropospheric tritium concentrations in the Great Basin-Wasatch Range area include the so called 'spring leak', thunderstorms, and near surface evaporation. The spring leak occurs in the spring time when the tropopause breaks down between 30^{o} N and 60^{o} N and permits the mixing of troposphere air with tritium rich stratosphere air (Michel et al., 2018). Elevated tritium deposition is also associated with summer thunderstorm thunderheads that penetrate the troposphere and bring down precipitation with elevated ^{3}H concentrations. Evaporation and atmospheric exchange of inland surface water and saturated soil with elevated tritium can also increase inland tritium deposition. Evaporation peaks in the spring and summer. The consequence of these processes combined with the variability in storm track trajectories results in the wide range of ^{3}H concentrations in modern precipitation. For example, spring and summer storm tracks crossing the Great Basin are subject to considerable precipitation and re-evaporation, and summer thunderstorms commonly involve the NAM.

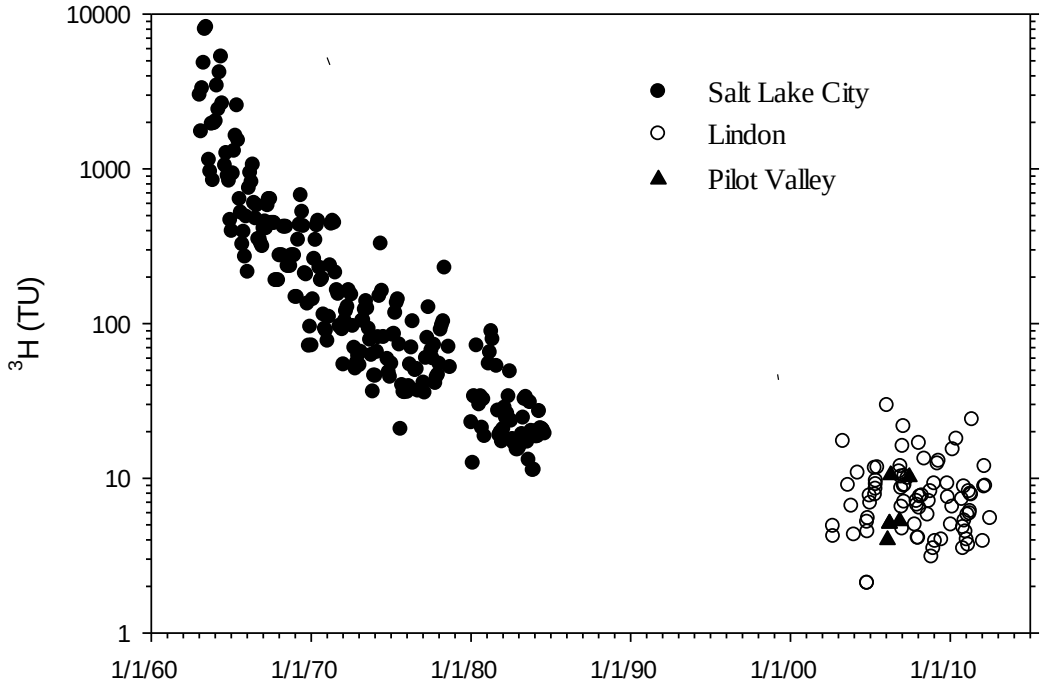

Fig. 8 Tritium concentrations in transition zone precipitation.

4.3 Stable Isotopes

The Lindon $\delta^{18}O$ data ranges from 3.36 to -28.18 ‰ with average and median values of -14.25 and -14.16 ‰, respectively. The $\delta^{2}H$ data ranges from 7 to -215.4 ‰ with average and median values of -107.74 and -107.0 ‰, respectively. The stable isotopic data for all three stations have been plotted relative to the GMWL (Fig. 10). Local meteoric water lines (LMWL) calculated for each data set and for the cumulative data are:

$$\text{Pilot Valley } \delta^{2}H = 7.0\ \delta^{18}O - 14 \text{ ‰} \quad (2)$$

$$\text{Lindon } \delta^{2}H = 7.2\ \delta^{18}O - 5.1 \text{ ‰} \quad (3)$$

$$\text{Wasatch Plateau } \delta^{2}H = 8.7\ \delta^{18}O + 27.7 \text{ ‰} \quad (4)$$

$$\text{Cumulative data } \delta^{2}H = 7.0\ \delta^{18}O - 8.3 \text{ ‰} \quad (5)$$

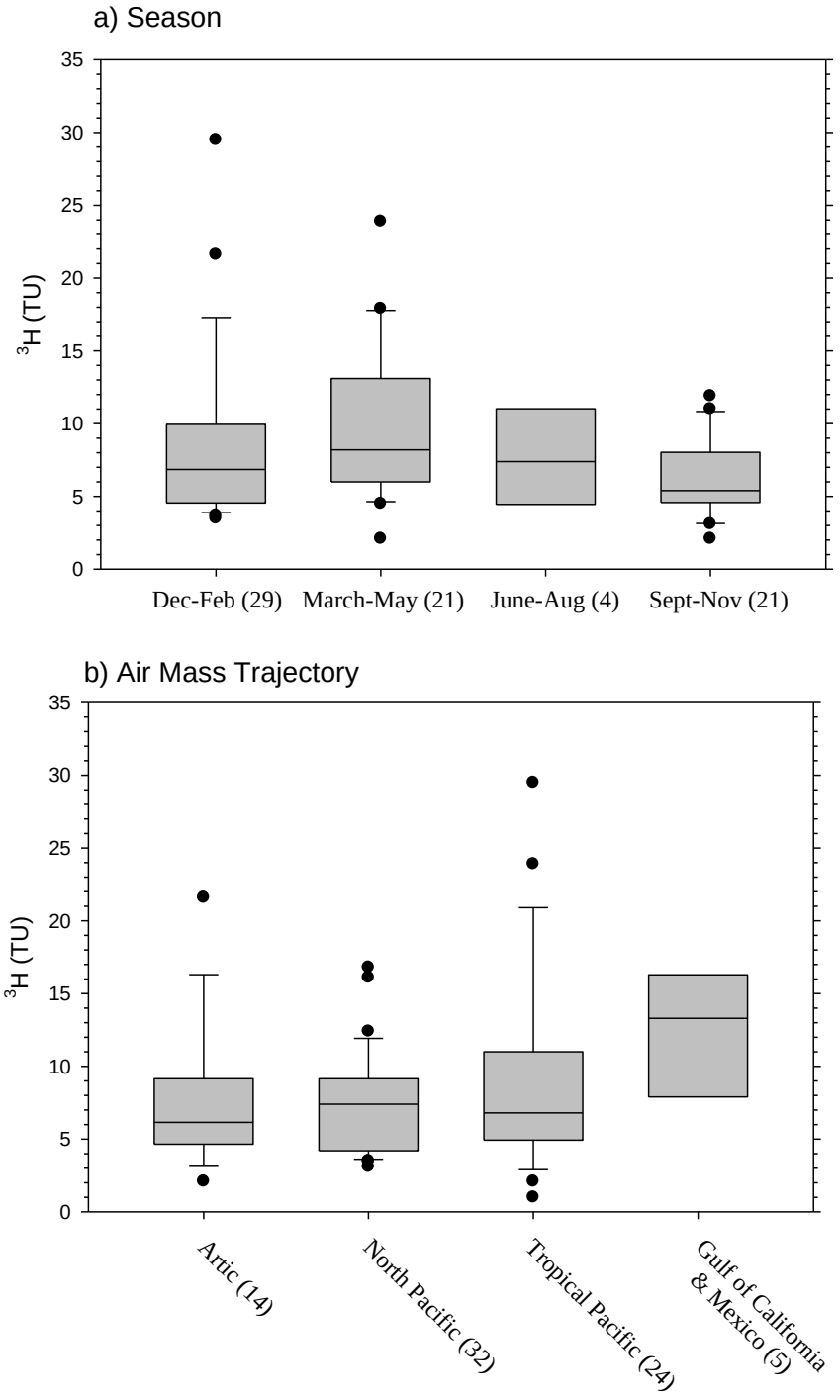

Fig. 9 Box plots of ^{3}H concentrations in Lindon precipitation organized by season (a) and storm track trajectory (b). The numerical values associated with the seasons and storm tracks are the number of samples. The line in the box is the median value (Q2 or 50th percentile), the top and bottom of the box are the 75th percentile (Q3) and the 25th percentile (Q1), and the bottom and top whiskers are Q1-1.5*IQR and Q3+1.5*1QR, respectively, where IQR is the 25th to 75th percentile. Outliers are shown as filled circles.

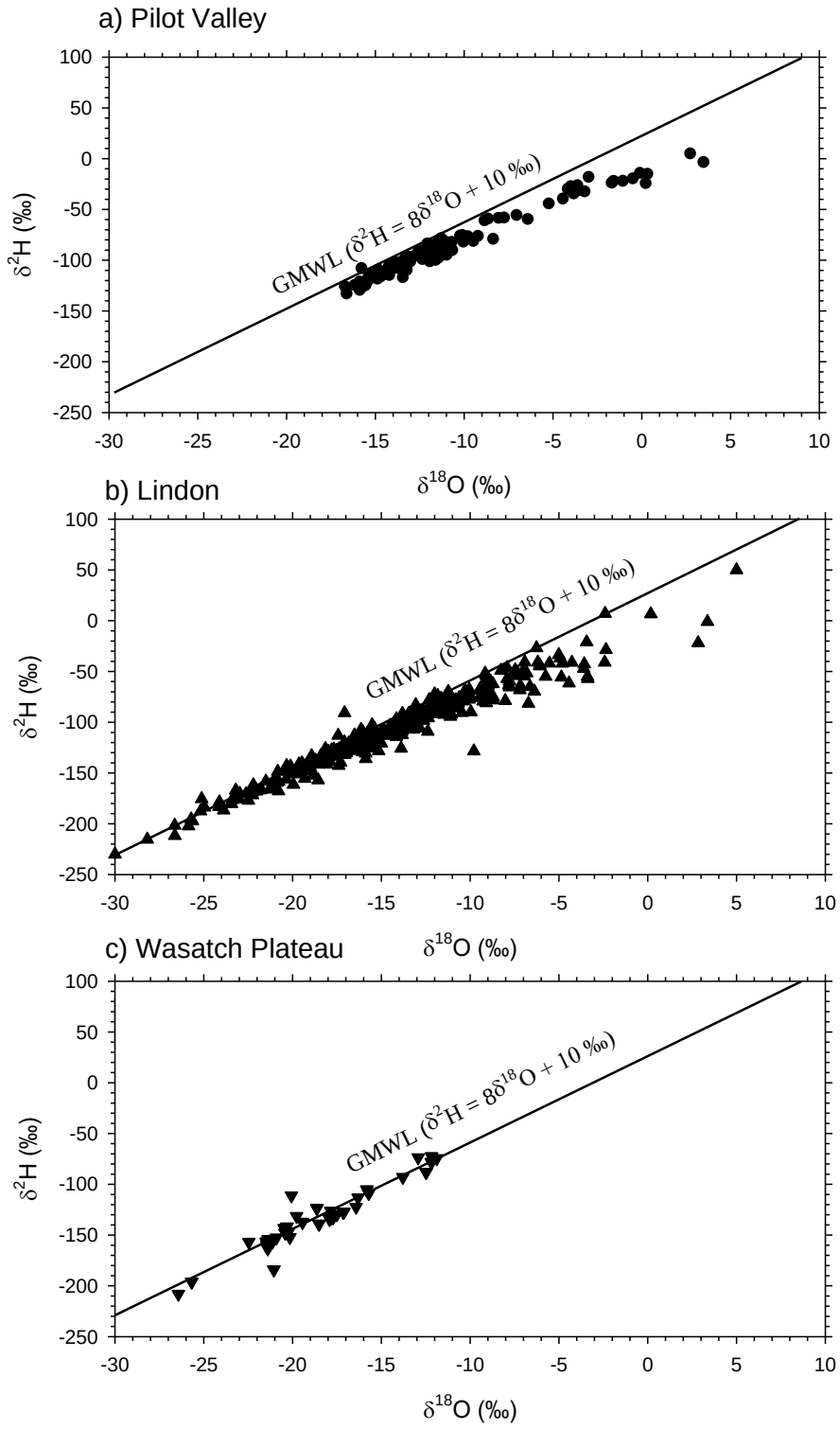

346

347 Fig. 10 Pilot Valley (a), Lindon (b) and Wasatch Plateau (c) precipitation stable isotopic
348 compositions plotted relative to the GMWL.

349

Although the LMWL's differ from the GMWL, there are no statically significant differences between the Lindon and Wasatch Plateau data relative to the GMWL. The p values for the GMWL vs. Lindon and Wasatch data are 0.2923 and 0.4348, respectively. What this means is that the GMWL is a reasonable surrogate for Wasatch Front and Wasatch Range precipitation.

Pilot Valley precipitation differs significantly from the GMWL with a p value of 0.0231. Much of the Pilot Valley data plots subparallel to the GMWL, and the data with values > -11 ‰ in (> -78 ‰ δ^2H) plot along a possible evaporation trajectory (Fig 10a). A similar apparent evaporation trend occurs in the Lindon data (Fig. 10b). The percentage of Lindon and Pilot Valley precipitation that has been subjected to partial evaporation (i.e., $\delta^{18}O$ > -11 ‰) are 24 and 30 percent, respectively. Partial evaporation of precipitation begins in late spring and continues through early fall (Fig. 11). By summer when the air is warmer, thunderstorms are common, and the NAM begins about half of the Lindon precipitation and all of the Pilot Valley precipitation has undergone some evaporation. The evaporative signatures are attributed to the partial evaporation of rain droplets accompany the free fall of rain. In the summer and early fall it is not uncommon for rain to completely evaporate before reaching the ground (virga effect). Partial evaporation in the Great Basin has been reported by Friedman et al. (2002b). The subparallel plotting of the Pilot Valley data is attributed to the combined factors of isotopic fractionation accompanying rain out and the contributions from multiple episodes of re-evaporation and subsequent re-precipitation of soil moisture as storms cross the Great Basin.

In addition to the partial evaporation several trends are apparent when the Lindon data are plotted relative to month, season, and storm track (Fig. 12). Median δ^2H values are most negative in the winter (December - February) and early spring (March) and become less negative in the late spring through fall (April-October; Fig. 12a). Except for winter vs. spring all of the seasonal data are statistically different from each other. The spring data are skewed toward more negative values (Fig. 12b). When March is not included with April and May the spring time data is statistically different than the winter data. Storm track median δ^2H precipitation values become heavier from the Artic to the Gulf of California-Gulf of Mexico (Fig.12c). The Gulf of California-Gulf of Mexico trajectory precipitation data are statically heavier than all other air trajectory data. The less negative values caused by rain droplet partial evaporation is the result of warm, late spring and summer tropical Pacific and Gulf of California-Gulf of Mexico air (Fig.

380 4). About 50 percent of Lindon winter precipitation is associated with very cold cloud
381 conditions (i.e., $\delta^{18}O$ < ~-17 ‰). Between April and October, when Artic and north Pacific air
382 trajectory storm are less frequent, all of the Lindon precipitation $\delta^{18}O$ is > -17 ‰.

383

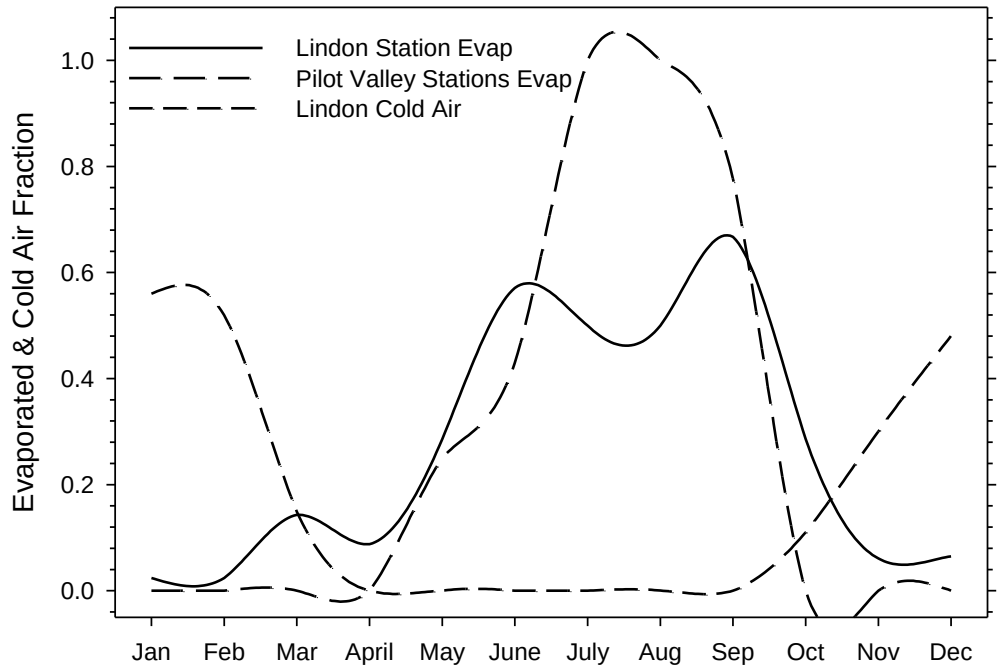

384

385 Fig.11 Fraction of precipitation that is partially evaporated and that formed during very cold
386 cloud conditions. Evaporation = $\delta^{18}O$ > -11‰ and cold cloud = $\delta^{18}O$ < -17 ‰.

387

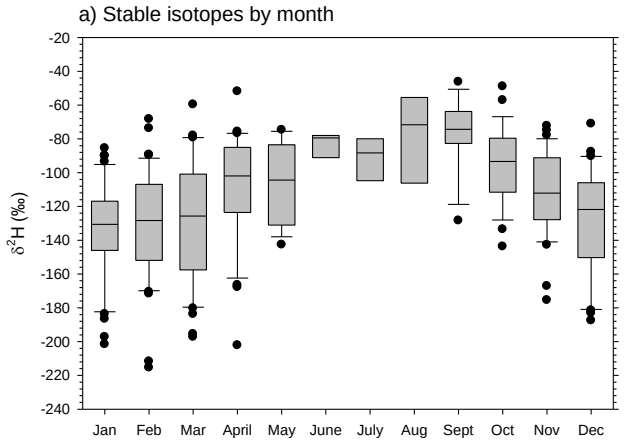

388

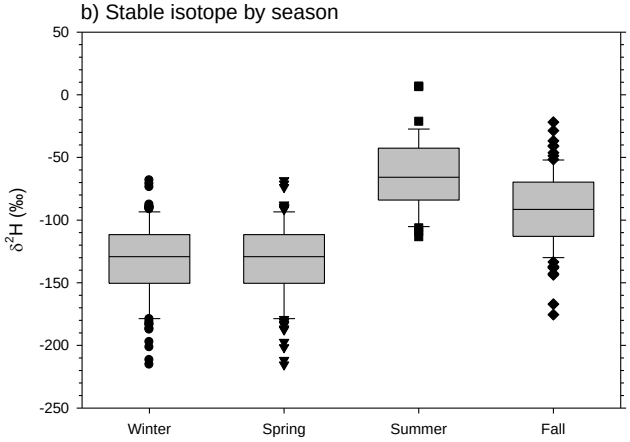

389

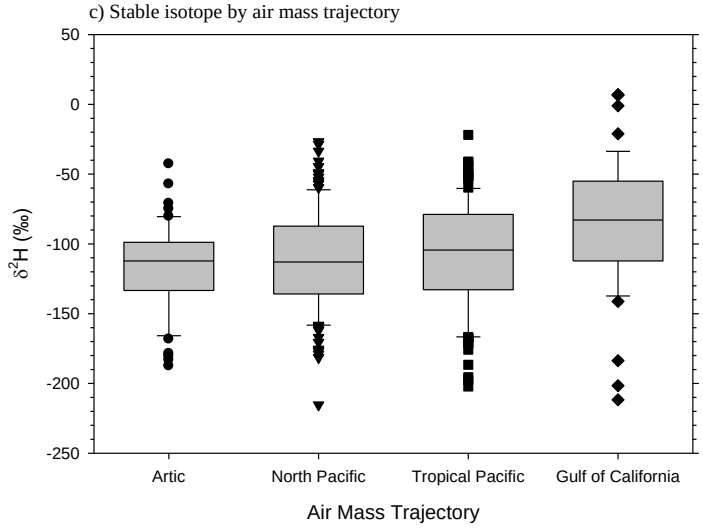

390

391 Fig. 12 Box plots of Lindon δ^2H data organized by month (a), season (b) and air mass trajectory
392 (c).

5 Conclusions

The Wasatch Range forms a physiographic and orographic barrier that has a profound impact on the oceanic air mass trajectories that cross the interior of the southwestern United States. The southeast flowing cold Artic air, west flowing cool North Pacific Ocean air, and northeast flowing tropical Pacific Ocean air originate in the Pacific Ocean 1,000 to 1,500 km from the Wasatch Range. North flowing Gulf of California-Gulf of Mexico air originates in the Gulf of California and Gulf of Mexico 1,000 to 2,000 km away. The percentage of storm carrying air mass that reaching the base of the Wasatch Range vary by source area and season. When the air masses reach the Wasatch Range the north and south flowing air is partially funneled along the range front.

In the study area the Oceanic Niño Index (ONI) is not a reliable predictor of precipitation flux or for use as a standalone tool for assessing precipitation isotopic composition. The lack of correlation between the ONI index with transition zone precipitation or isotopic composition is likely influenced by the north-south migration of the ENSO Dipole (aka North American Dipole). Coupling of the ENSO Dipole with other Pacific Ocean atmospheric and SST oscillations shifts the ENSP Dipole north and south. The varying durations of wet and dry cycle are like related to this migration.

The flow of moisture from the ocean sources to the continental interior results in tritium enrichment and stable isotopic depletion. Modern tritium deposition averages 8.5 TU and ranges between 2.1 and 29.5TU. Average tritium concentrations are greater in the spring time and from storms associated with tropical Pacific and Gulf of California-Gulf of Mexico air. Elevated tritium deposition is associated with the so called ‘spring leak’, thunderstorms, and land surface evaporation. These processes combined with the variability in storm track trajectories results in modern precipitation having a wide range of tritium concentrations.

Local meteoric water lines (LMWL) for the Lindon station and the cumulative LMWL are:

$$\text{Lindon } \delta^{2}H = 7.2\ \delta^{18}O - 5.1‰$$

Cumulative data $\delta^2H = 7.0\ \delta^{18}O - 8.3‰$

Although the LMWL's differ from the GMWL, there are no statically significant differences between the Lindon and cumulative LMWL's and the GMWL, thus the GMWL can be used as a reference for surface and groundwater investigations. Most winter precipitation is isotopically depleted relative to precipitation falling the rest of the year. The depleted isotopic signatures are attributed to the cold, winter cloud temperatures. About 25 to 30 percent of the precipitation is seasonally evaporated. The evaporative signatures are due to the partial evaporation of rain droplets accompany the free fall of rain. Great Basin precipitation plots sub-parallel to the GMWL. The subparallel plotting is attributed to the combined factors of isotopic fractionation accompanying gradual rain out and the multiple episodes of re-evaporation and subsequent re-precipitation of soil moisture as storms cross the numerous Great Basin mountain ranges.

6 Acknowledgments

This research was supported by the Brigham Young University Laboratory of Isotope Hydrogeology.

7 References Cited

Araguás, L., Froehlich, K. & Rozanski, K. (1998). Stable isotope composition of precipitation over southeast Asia. J. Geophy. Res. 103 (D22), 28721–28742.

Benson, L. (2017). Great Basin surface water and precipitation isotopic data. https://digitalcommons.unl.edu/cgi/viewcontent.cgi?article=1001&context=usgsdata, accessed 2/12/21

Benson, L. & Klieforth, H. (1989). Stable isotopes in precipitation and ground-water in the Yucca Mountain region, southern Nevada: Paleoclimatic implications, in Aspects of Climate Variability in the Pacific and Western Americas. Geophys. Monogr. Ser., 55, 41-59.

Benjamin, L., Knobel, L.L., Hall, L.F., Cecil, L.D. & Green J.R. (2004). Development of a local meteoric water line for southeastern Idaho, western Wyoming, and south-central Montana. U.S. Geol. Surv. Sci. Inv. Rpt. 2004-5126, 17 p.

Bowen, G.J. (2008). Spatial analysis of the intra-annual variation of precipitation isotope ratios and its climatological corollaries. J. Geophy. Res., 113, D05113. doi:10.1029/2007JD009295

Brown, D. P. (2011). Winter circulation anomalies in the western United States associated with antecedent and decadal ENSO variability. Earth Interact. 15. doi:10.1175/2010EI334.1.

Cai, Z., & Tian, L. (2016) .Atmospheric controls on seasonal and interannual variations in precipitation isotope in East Asian Monsson region: Atmospheric controls on seasonal and interannual variations in the precipitation. Am. Meteor. Soc. http://dx.doi.org/10.1175/JCLI-D-15-0363.1

Clark ID, Fritz P. (1997). Environmental Isotopes in Hydrogeology. CRC press: Boca Raton.

Craig, H., (1961). Isotopic variations in meteoric waters. Sci., 133, 1702-1703.

Craig, H., Boato, G. & White, D.E. (1956). Isotopic geochemistry of thermal waters: Nat. Acad. Sci. Nucl. Sci. Ser. Rep 19, 29-36.

Cross, M., McGee, D., Broecker, W. S., Quade, J., Shakun, J. D., Cheng, H., Lu, Y. & Edwards, R. L. (2015). Great Basin hydrology, paleoclimate, and connections with the North Atlantic: A speleothem stable isotope and trace element record from Lehman Caves, NV. Quat. Sci. Rev. 127, 186-198. doi.org/10.1016/j.quascirev.2015.06.016

Danasgaard, W. (1953). The abundance of O18 in atmospheric water and water vapour. Tellus, 5, 461-469.

Danasgaard, W. (1954). The abundance of O18 in fresh water. Geochim. et Cosmochim. Acta, 6, 241-260.

Dansgaard, W. (1961). The isotopic composition of natural waters with special reference to the Greenland Ice Cap. Medd. Groenland, 165, (2), 120 p.

Dansgaard, W. (1964). Stable isotopes in precipitation. Tellus, 6, 435-468.

Dobrowski, S. Z., Abatzoglou, J. T., Greenberg, J. A. & Schladow, S. G. (2009). How much influence does landscape-scale physiography have on air temperature in a mountain environment? Agric. For. Meteorol. 149, 1751-1758. doi: 10.1016/j.agrformet.2009.06.006

Duan, W., Ruan. J., Luo, W., Li., T., Tian, L., Zeng, G., et al. (2016). The transfer of seasonal isotopic variability between precipitation and drip water at eight caves in the monsoon regions of China. Geochim. et Cosmochim. Acta, 15, 250-266.

Easto, C.J. & Dettman, D.L. (2016). Isotope effects in hydrogeologic and climate reconstructions of monsoon climates: Implications of some long-term data sets for precipitation. Chem. Geol., 430, 78-89.

Ehhalt, D., Knot, K., Nagel, J.F. & Vogel, J.C. (1963). Deuterium and oxygen 18 in rain water. J. Geophys. Res., 68, 3775-3780.

Epstein, S. (1956). Variations of the O18/O16 ratios of fresh water and Ice. Nat. Acad. Sci., Ncl. Sci. Rep., 19, 20-25.

Epstein, S., & Mayeda, T. (1953). Variation on 18O content of waters from natural sources. Geochim. et Cosmochim. Acta, 4, 213-214.

Friedman, I. (1953) Deuterium content of natural waters and other substances. Geochim. et Cosmchim. Acta, 4, 89-103.

Friedman, I., G. I. Smith, J. Gleason, A. Warden, & J. M. Harris (1992). Stable isotope composition of precipitation in southeastern California, 1, Modern precipitation. J. Geophys. Res., 97, 5795-5812.

Friedman, I., Harris, J.M., Smith, G.I., Craig A. & Johnson, C.A. (2002a). Stable isotope composition of waters in the Great Basin, United States 1. Air-mass trajectories. J. Geophy. Res. Atmos., 107, (19). doi:10.1029/2001JD000565

Friedman, I., Smith, G.I., & Johnson, C.A., and Moscati, R.J. (2002b). Stable isotope composition of waters in the Great Basin, United States, 2, Modern precipitation. J. Geophys. Res., 107, (19), doi: 10.1029/2001JD000566.

Gat, J. (2001). Environmental isotopes in the hydrogeological cycle - Principles and applications. IAEA, 2, 235 p.

Gilfillan, E.S. Jr. (1934). The isotopic composition of sea water. J. Am. Chem. Soc., 56, 406-408.

Hager, G. & Foelsche, U. (2015). Stable isotope compositions of precipitation in Austria. Aust. J. Earth Sci., 108, (2), 2-13.

Harada, M. & Titani, T. (1935). Isotopic composition of rain and snow water. Chem. Soc. Japan, 10, 206-263.

Houghton, J. G. (1969). Characteristics of rainfall in the Great Basin. Desert Res. Inst., Univ. Nevada, Reno, Pub. 41054, 205 p.

Houghton, J.G. (1979). A model for orographic precipitation in the north-central Great Basin. Monthly Weath. Rev., 107, 1462-1475.

IAEA (2021). Global network of isotopes in precipitation (GNIP). https://nucleus.iaea.org/wiser, accessed March 21, 2021.

Jeton, A.E., Watkins, S.A., Lopes, T.J. & Huntington, J. (2005). Evaluation of Precipitation Estimates from PRISM for the 1961-1990 and 1971-2000 Data Sets, Nevada. U.S. Geol. Surv. Sci. Invest. Rpt. 2005-5291, 35 p.

Klaus, J., Mcdonnell, J., Jackson, R.C. & Griffiths, N. (2015). Where does stream water come from in low-relief forested watersheds? A dual-isotope approach. Hydrol. Earth Syst. Sci., 19, (1), 125-35.

Kobayakawa, H.Y. & Horibe, Y. (1960). Deuterium abundance of natural waters. Geochim. et Cosmochim. Acta, 20, 273-283.

Kurita, N., Fujiyoshi, Y., Nakayama, T., Matsumi, Y. & Kitagawa, H. (2014). Atmospheric circulation controls on the inter-annual variability in precipitation isotope ratio in Japan. Climate Past Disc., 10 (5), 3989-4032.

Lewis, G.N. & Cornish, R. (1933). Separation of the isotopic forms of water by fractional distillation. J. Am. Chem. Soc., 55, 5061-5062.

Mantura, N.J. & Hare, S.R. (2002). The Pacific-Decadal Oscillation. J. Ocean., 58, 35-44.

McEvoy, D.J., Mejia, J.F. & Huntington, J.L. (2014). Use of an observation network in the Great Basin to evaluate gridded climatic data. J. Hydrometeor., 5 (5) 1913-1931. doi.org/10.1175/JHM-D-14-0015.1

Merlivant, L. & Jouzel, J. (1979). Global climatic interpretation of the deuterium-oxygen 18 relationship for precipitation. J. Geophys. Res, 84. 5029-5033.

Michel, R.L., Jurgens, B.C. & Young, M.B. (2018). Tritium deposition in precipitation in the United States, 1953-2013. US Geol. Surv. Sci. Invest. Rpt. 2018-5086, 12 p.

NOAA (2021). HYSPLIT a Hybrid Single-Particle Lagrangian Integrated Trajectory model. www. noaa.gov/HYSPLIT_traj.php, accessed March 10, 2021.

Pape, J.R., Banner, J.L., Mack, L.E., Musgrove, M. & Guilfoyle, A. (2010). Controls on oxygen isotope variability in precipitation and cave drip waters, central Texas, USA. J. Hydrol., 385, 203-215.

Patrick, N. (2014). Evaluating near surface rates over complex terrain using an embedded micrologger sensor network in Great Basin National Park. Ohio State University.

Rozanski, K., Araguas, L. & Gonfiantini, R. (1993). Isotopic patterns in modern global precipitation, climate change in continental isotopic record. Geophys. Monogr, 78, 1–37.

Schell, W.R., Sauzay, G. & Payne, B.R. (1970). Tritium injection and concentration distribution in the atmosphere. J. Geophy. Res. 75 (12), 2251-2266. https://doi.org/10.1029/JC075i012p02251

Siegenthaler, U. & Oeschger, H. (1980) .Correlation of 18O in precipitation with temperature and altitude. Nature, 285, 314-317.

547 Smith, K., Strong, C. & Shih-Yu Wang, S-Y (2015). Connectivity between historical Great
548 Basin precipitation and Pacific Ocean variability: A CMIP5 Model Evaluation. J.
549 Climate, 28, 15, 6092-6112. doi.org/10.1175/JCLI-D-14-00488.1

550 Smith, G. I., Friedman, I., Gleason, J. & Warden, A. (1992). Stable isotope composition of
551 ground waters in southeastern California, 2, Ground waters and their relation to modern
552 precipitation. J. Geophys. Res., 97, 5813-5823

553 Suess, H.E. (1970). Transfer of carbon 14 and tritium from the atmosphere to the ocean. J.
554 Geophy. Res., 75 (12), 2363–2364. https://doi.org/10.1029/JC075i012p02363.

555 Tes, R.V. (1939). Isotopic composition of rain water. Akad. Nauk, USSR, 23. 674.

556 Vuille, M. & Werner, M. (2005). Stable isotopes in precipitation recording South American
557 summer monsoon and ENSO variability: observations and model results. Climate Dyn.
558 25 (4), 401-413.

559 Yurtsever, Y. (1975). Worldwide survey of isotopes in precipitation. IAEA report, Vienna.

560 Wang, S.-Y., Gillies, R.R. & Reichler, T. (2012). Multidecadal drought cycles in the Great Basin
561 recorded by the Great Salt Lake: Modulation from a transition-phase teleconnection. J.
562 Climate, 25, 1711-1721. doi:10.1175/2011JCLI4225.1.

563 WRCC (2021). Western Regional Climate Center. https://wrcc.dri.edu/summary/Climsmut.html,
564 accessed February 18, 2021.

565 Wise, E. K. (2010). Spatiotemporal variability of the precipitation dipole transition zone in the
566 western United States. Geophys. Res. Let. 37, L07706. doi:10.1029/2009GL042193

567 Yeh, H., Lin, H., Lee, C., Hsu, K. & Wu, C. (2014). Identifying seasonal groundwater recharge
568 using environmental stable isotopes. Hydrology, 6, 203-215.